Directionality bias is necessary to explain spatiotemporal progression of pathology in mouse models of tauopathy

Justin Torok[1], **Christopher Mezias**[2], **Ashish Raj**[1*]

***For correspondence:**
ashish.raj@ucsf.edu (AR)

[1]University of California at San Francisco, Department of Radiology; [2]Cold Spring Harbor Laboratory, Department of Neuroscience

Keywords
Tau; protein pathology; Alzheimer's Disease; tauopathy; neurodegenerative disease; mouse models; mathematical modeling; network spread models

Abstract Mounting evidence implicates trans-synaptic connectome-based spread as a shared mechanism behind different tauopathic conditions, yet also suggests there is divergent spatiotemporal progression between them. A potential parsimonious explanation for this apparent contradiction could be that different conditions incur differential rates and directional biases in tau transmission along fiber tracts. In this meta-analysis we closely examined this hypothesis and quantitatively tested it using spatiotemporal tau pathology patterns from 11 distinct models across 4 experimental studies. For this purpose we developed and employed the NexIS:dir, a mathematical model that extends previous work by incorporating net directionality. Our data unambiguously supports the directional transmission hypothesis. First, retrograde bias is an unambiguously better predictor of tau progression than anterograde bias. Second, while spread exhibits retrograde character, the best NexIS:dir models incorporate the mixed effects of both retrograde- and anterograde-directed spread, with notable tau-strain-specific differences. We also found a nontrivial association between directionality bias and tau strain aggressiveness, with more virulent strains exhibiting less retrograde character. Taken together, our study implicates directional transmission bias in tau transmission along fiber tracts as a general feature of tauopathy spread and a strong candidate explanation for the diversity of spatiotemporal tau progression between conditions. This simple and parsimonious mechanism may potentially fill a critical gap in our knowledge of the spatiotemporal ramification of divergent tauopathies.

Introduction

It is well known that the spatiotemporal pattern of Alzheimer's disease (AD) pathology development is characterized by stereotyped progression. Braak & Braak were the first to describe the staging of hallmark neurofibrillary tangles (NFT) of misfolded tau protein: these are first detected in the entorhinal cortex (EC) and locus coeruleus (LC), followed by limbic areas and then neocortical areas while sparing primary sensorimotor cortices ***Braak and Braak*** (***1991***). Identifying the causal mechanisms that govern why tau follows this characteristic spreading pattern in AD is a longstanding goal of neurodegenerative disease research. Progress on this front has rapidly advanced with the discovery that hyperphosphorylated tau undergoes intercellular spread following axonal trans-

port and trans-synaptic transmission ***Ahmed et al.*** (***2014***); ***Clavaguera et al.*** (***2009***); ***Holmes et al.*** (***2014***); ***Tai et al.*** (***2014***)).

However, key aspects of the transmission process remain unknown, especially whether axonal tau travels bidirectionally or preferentially in either in the same direction (anterograde) or in the reverse direction (retrograde) with respect to the neuron's polarity. Similarly, it is not known whether the trans-synaptic transmission occurs from post- to pre-synapse, post- to pre-synapse, or some mixture of the two. Much phenomenological evidence and descriptive studies are now available to support both anterograde and retrograde transmission ***Wu et al.*** (***2013***); ***Langer Horvat et al.*** (***2023***). However, these studies do not provide a statistically rigorous support to net directionality across multiple disease models, nor do they allow inference of the net directional bias in those cases where it may not be either fully anterograde or retrograde. Most importantly, current evidence lacks the ability to tie directional bias to more fundamental processes in the aggregation and transmissions of tau along axons.

The purpose of this study is to assess whole-brain and unbiased statistical support for net directionality gleaned from integrated large-scale meta-analysis of all available tauopathic data measured in our chosen model system - transgenic mouse models of AD tauopathy. We hope to move beyond current evidence that has understandably come from descriptive, hypothesis-driven mechanistic experimental bench or animal studies. These studies, based on selected brain structures or selected tau conformers or strains, are difficult to generalize and frequently produce conflicting results. Instead we aim for "big picture" and generalizable statistical evidence that together supports the emergence of directional bias in tau transmission. We achieve these goals by analysing histological tau data from 4 individual studies comprising 11 experimental conditions, all of which use P301S-tau-expressing mice***Boluda et al.*** (***2015***); ***Hurtado et al.*** (***2010***); ***Iba et al.*** (***2013***); ***Kaufman et al.*** (***2016***), to perform a meta-analysis of mouse tauopathy at a whole-brain level in the context of network spread of tau.

We approached this task in two distinct ways. First, we employed statistical and graph theoretical techniques to generate evidence for directional bias in tau spread, and report that indeed empirical data cannot be explained without introducing directionality of transmission. Second, we used novel mathematical models of tau network spread, which enabled us to explore directional bias in the context of other key pathological processes, such as accumulation of tau. In particular, we investigated whether intrinsic net directional bias in trans-synaptic spread can better recapitulate empirical pathology data. For this purpose, we used as our base model our previous mathematical network transmission (NT) models of pathology spread along anatomical connectivity successfully recapitulate the spatiotemporal regional volumetric loss in patients' brains. These models show great promise in predicting later disease patterns from early timepoints ***Raj et al.*** (***2012***, 2015); ***Zhou et al.*** (***2012***); ***Iturria-Medina*** (***2013***); ***Weickenmeier et al.*** (***2018***); ***Bertsch et al.*** (***2023***).

The specific mechanistic model we employed is an extension of the NexIS:global model of pathology spread ***Anand et al.*** (***2022***), expanded to incorporate directionally biased transmission in both anterograde (pre- to post-synaptic) or retrograde (post- to pre-synaptic) directions. This model has previously been shown to more accurately recapitulate the longitudinal progression of tauopathy in mouse models than prior network transmission models ***Raj et al.*** (***2015***). We call this model *NexIS:dir*. The model is simulated on the mesoscale connectome of the mouse, utilizing the Allen Mouse Brain Connectivity Atlas (AMBCA), which not only provides connection strengths between region-pairs but also the directionality of those connections ***Oh et al.*** (***2014***). This model-based method of studying connectivity and directionality has the advantage of not depending on transmission along a single projection, but incorporates directional transmission across the entire brain network.

Our results several previously unknown and striking findings. **1)** First, NexIS:dir models using fully retrograde bias in tau transmission universally outperform those using fully anterograde bias across all tauopathy models. **2)** Second, the retrograde bias is conformation- and transgene

background-dependent, thus confirming that differential directional biases can effectively recapitulate divergent spatiotemporal tau progression patterns observed in various transgenic mouse models of tauopathy. **3)** Peak performance for mouse models exhibiting prominent net retrograde bias is achieved a mixed model of retrograde and anterograde biases rather than purely retrograde or nondirectional models of spread. **4)** We found striking associations between global accumulation rate, global spread rate, and net directionality bias across all mouse models. This finding leads to propose an underlying interaction model between these distinct phenomena, whereby more aggressive tau strains exhibit both higher accumulation and spread rates but *lower* net directionality bias.

Overall, we found that the aggressiveness of tau accumulation and transmission, combined by directionally biased spread, can provide a parsimonious model of tau progression.

Results

Analysis of directed connectivity graph indicates retrograde preference of tau migration

Previous network modeling has demonstrated that connectivity with afflicted regions drives subsequent spatiotemporal tau progression, but was limited to undirected connectomes ***Mezias et al.*** (***2017***); ***Raj et al.*** (***2012***, 2015); ***Zhou et al.*** (***2012***); ***Weickenmeier et al.*** (***2018***); ***Iturria-Medina*** (***2013***). This mimics a diffusion process whereby the direction of tau spread between region pairs is dictated only by the concentration difference between them. However, migration of tau along axonal projections is known to have both diffusive and active transport components ***Scholz and Mandelkow*** (***2014***), where molecular motors traffic cellular cargoes, including tau, asymmetrically between the soma and the axon terminal (**Figure 1A**). At a network level, this manifests as a *directionality bias*, with tau preferentially migrating in the *anterograde* (from presynaptic to postsynaptic regions, following the polarity of the projections) or *retrograde* (against the polarity of the projections) (**Figure 1B**). Exploring directionality requires the use of a *directed* connectome, which has been previously determined using viral tracing methods in wild-type mice by the Allen Institute for Brain Science (AIBS) ***Oh et al.*** (***2014***); here, we use a 426-region, bilateral version of the Allen Mouse Brain Connectome Atlas (AMBCA) (**Figure 1C**). This makes mouse models of tauopathy an ideal substrate for exploring the question of directional bias in tau spread. For this study, we utilized 11 distinct mouse models, whose descriptions can be found in **Table 1**). Of particular note is that 10 of 11 studies had the same genetic background (PS19), and therefore any differences between studies' tau pathology can be attributed to differences in seeding location and the molecular properties of the tau strain injected.

We first explored directional bias in a model-free way. **Figure 1D** shows the associations between end-timepoint tau pathology for the "IbaStrInj" mouse model ***Iba et al.*** (***2013***), which was quantified at 9 months post injection (MPI), and the connectivity from (*left panel*) and to (*right panel*) the seeded regions (in this case, the caudoputamen and primary motor cortex). We observed a strongly statistically significant association with respect to incoming connectivity to the seeded regions (Pearson's $R = 0.33$, $p < 0.001$), but not outgoing connectivity (R = 0.06, n.s.). Because preferential spread along incoming connections indicates that tau is migrating from postsynaptic to presynaptic regions, these results suggest that the IbaStrInj mouse model exhibits a net retrograde directionality bias.

We found that this appears to be a general feature of mouse tauopathy for the 11 models we explored, albeit with significant heterogeneity between studies and timepoints, as assessed by three different sets of graph metrics: connectivity from/to seed, out- and in-degree, and the first eigenvectors of the retrograde and anterograde Laplacian matrices (L_{ret} and L_{ant}, respectively; see also **Materials and Methods**) (**Figure 1E**). While the distributions of R values were all significantly above 0 by one-sample t-test following Fisher's R-to-z transformation (all $p < 0.01$), we found statistically significant differences within each pair of metrics. Specifically, associations with tau pathology

were greater for incoming rather than outgoing connectivity with seeded regions; for out-degree rather than in-degree; and for v_1 of L_{ret} rather than v_1 of L_{ant} (all $p < 0.001$ by two-sample t-test). Because out-degree and v_1 of L_{ret} are both associated with *positive* flows occurring from region j to region i along connection c_{ij} (see **Materials and Methods**), these results are consistent with retrograde-biased spread.

To examine these effects qualitatively, we returned to the end-timepoint pathology of the IbaStrInj mouse model and utilized a glass brain visualization of regional tau densities alongside the top 10% of connections from and to seeded regions (**Figure 1F**). We observed that many of the strongest projections from the primary motor cortex (MOp, orange sphere) terminate in the contralateral telencephelon and ipsilateral hindbrain (*top panel*, blue boxes), where this mouse model exhibits low pathology, as well as ipsilateral telencephalic regions, where pathology is higher. Therefore, we would expect the marginal association between outgoing connectivity and IbaStrInj pathology shown in **Figure 1D**. By contrast, incoming connectivity to both the MOp and caudoputamen (CP) is largely ipsilateral and originates in forebrain regions that exhibit high tau density. Overall, these results suggest that there is a retrograde rather than anterograde preference in mouse tauopathy.

NexIS:dir modeling of tau pathology in IbaStrInj demonstrates moderately but not wholly retrograde spread

To model the spread of tau more directly, we utilized the NexIS:dir model, an extension of the previously explored NexIS:global model ***Anand et al.*** (***2022***). This model, designed for directed connectomes like the AMBCA, proposes that directionality bias may have anterograde and retrograde components, which is represented by the directionality bias parameter s. Mathematically, s weights the spread along L_{ret} versus L_{ant}, with $s = 1$ indicating purely retrograde spread, $s = 0$ indicating purely anterograde spread, and $s = 0.5$ indicating nondirectional spread, which is equivalent to spread along the symmetrized connectome $C_{sym} = \frac{C+C^T}{2}$ (see **Materials and Methods** for more details). We postulated that, while spread may be net retrograde (**Figure 1D–F**), the best model of tau progression would require capturing intermediate directionality biases through s.

Figure 2 shows glass brain representations of IbaStrInj pathology at 1, 3, and 9 MPI as well as the predictions of four different NexIS:dir models: 1) NexIS:fit-s, where s was fit alongside the accumulation (α) and spread (β) parameters; 2) NexIS:ret, where s was fixed to 1; 3) NexIS:ant, where s was fixed to 0; and 4) NexIS:nd, where s was fixed to 0.5. All model parameters were optimized utilizing all timepoints together (see **Materials and Methods**). We observed that the rapid dissemination of tau between 0 and 1 MPI in this mouse model was poorly captured by all four models. However, by the last quantified timepoint, NexIS:fit-s captured the highest number of relevant features in tau spread relative to all other models. According to this model, spread was predominantly, but not completely, retrograde, with an optimal s value of 0.78. Each of the other models where s was fixed underperformed in different ways. NexIS:ant, the worst model, could not fit the spread process at all and predicted that tau pathology remained in the seeded regions. NexIS:ret did capture the spread of tau to lateral neocortical regions observed in this mouse model, but showed little spread elsewhere. NexIS:nd was able to accurately predict the spread of tau to neocortical and forebrain subcortical regions; however, it overpredicted pathology in the ipsilateral and contralateral CP as well as the midbrain. NexIS:fit-s demonstrated a net decrease in pathology in the CP as well as spreading throughout lateral forebrain regions, with an excellent overall fit across all timepoints ($R = 0.56$, $p < 0.001$). Therefore, we conclude that, in order to truly predict the spatiotemporal deposition of tau in IbaStrInj, we require the precise quantification of the proportion of directionality bias through s.

NexIS:dir demonstrates that intermediate retrograde bias is the best overall model of tau spread across all studies

We extended the above analysis for IbaStrInj across all 11 mouse tauopathy models to explore if there were any trends in directionality bias. **Figure 3A** shows R-t curves for the four NexIS:dir models, where each colored line represents the association between end-timepoint pathology (dashed black lines; see **Figure S1** for illustrations of the observed end-timepoint tau pathology for all 11 models) and the each model's predicted distributions across the relevant time range. We also display the optimal s parameters for the NexIS:fit-s models (see also **Table 1**). While NexIS:nd and NexIS:fit-s often performed equivalently well, as exhibited by $s_{opt} \approx 0.5$, NexIS:ret also exhibited good agreement and invariably outperformed NexIS:ant. As in **Figure 2**, all parameters were fit longitudinally for this analysis.

To delve into the performance in more detail, we obtained overall R values as well as R values at each quantified time point for all four models, where parameters were longitudinally fit as above (**Figure 3B**). Overall, while NexIS:fit-s is always the superior model given that it optimizes the s parameter, NexIS:nd is most frequently the second-best model across studies. NexIS:ret, however, outperforms it for IbaStrInj and BoludaDSAD, and as well as at certain timepoints for other studies (e.g., Hurtado). NexIS:ant is unequivocally the least predictive model across all studies. We also assessed overall directional bias using two metrics: 1) overall ΔR_{dir} (i.e., the difference between R_{ret} and R_{ant} per study, which are plotted as blue and purple squares in **Figure 3B**, respectively); and 2) s_{opt}, the optimal s value for NexIS:fit-s. Both metrics were statistically significantly retrograde by one-sample t-test, with ΔR_{dir} being highly statistically significant (**Figure 3C**).

We also examined an alternative fitting scheme, where we fit the β (spread rate) and s parameters at each timepoint individually after fixing α to its longitudinally fit value. This choice was motivated by the fact that α, as the global accumulation parameter, captures the increase in overall pathology burden and is best determined using all timepoints together (see **Materials and Methods**). Model performance generally followed those obtained using longitudinal fitting, with some subtle differences (**Figure 3D**). For instance, NexIS:ret exhibited a higher mean R across timepoints for the Hurtado study than NexIS:nd, and NexIS:ant exceeded NexIS:ret performance for BoludaCBD. However, as with the longitudinally assessed bias metrics shown in **Figure 3C**, per-timepoint ΔR_{dir} and s_{opt} also showed a highly statistically significant retrograde tendency (**Figure 3E**). Therefore, NexIS:dir conclusively demonstrated that mouse tauopathy models appear to have a net retrograde as opposed to anterograde character, with variation between individual studies.

Spread rate, accumulation rate, and directional bias are mutually interdependent

Lastly, we postulated that the optimal values of three key NexIS:dir parameters (α, β, and s) may be correlated to each other. **Figure 4A–C** shows the linear regression between the per-timepoint fit values of each pair of parameters. Notably, s was negatively correlated with both β ($R^2 = 0.10$, $p < 0.05$) and α ($R^2 = 0.17$, $p < 0.01$) (**Figure 4A** and **B**, respectively). Of the three pairs of parameters, α and β actually showed the strongest overall correlation (**Figure 4C**, with an R^2 value of 0.24 ($p < 0.01$). This association was in the positive direction, which is consistent with the negative relationships observed for each parameter with respect to s. We also found that there was no temporal shift in the s parameter when fit per-timepoint (**Figure S2**). Therefore, we conclude that only strain identity, and to some extent seeding location, contributes to net directionality.

These results lead us to propose the following strain-specific model of mouse tauopathy. The pathogenicity of a particular tau strain, which can be assessed by either its rate of accumulation or its rate of spread throughout the brain, tends to contribute to both simultaneously. As these two processes are considered to be biologically distinct, the positive association between them is notable. By contrast, spread bias (in the retrograde direction) appears to be associated with less pathogenic tau strains. The implications of these findings are explored in the **Discussion** below.

Discussion

While prior studies have firmly established the predominance of trans-synaptic spread mechanisms in driving spatiotemporal pathology development in AD ***Ahmed et al.*** (***2014***); ***Boluda et al.*** (***2015***); ***Clavaguera et al.*** (***2009***); ***Holmes et al.*** (***2014***); ***Iba et al.*** (***2013***, 2015); ***Kaufman et al.*** (***2017***); ***Mezias et al.*** (***2017***); ***Raj et al.*** (***2012***), the present research is the first to explore whether the direction of trans-synaptic tau spread might be superior to non-directional spread, different across tau strains, injection sites, injectate types and genetic backgrounds. We used both statistical and mathematical modeling tools to interrogate the emergence of net directional bias in tau transmission across 11 transgenic mouse datasets.

Summary of key results

Our analyses revealed three previously unknown and striking findings. First, we found a notable net retrograde bias in network-based transmission of tau across all tauopathy studies, with anterograde-biased spread models exhibiting poor performance. Second, the retrograde bias is conformation- and seeding-site-dependent, and extrapolating the NexIS:dir mathematical model over the whole brain network led to divergent spatiotemporal tau progression patterns which quantitatively matched the study-specific observed tau. These data suggest that the diverse spatiotemporal presentation of tauopathic conditions ***Warren et al.*** (***2013***); ***Janelidze et al.*** (***2020***); ***Thijssen et al.*** (***2020***), might arise partly due to differential directional biases during trans-synaptic spread. Third, we found an unexpected interdependence of the NexIS:dir parameters across studies, with tau spread rate and accumulation rate being positively associated with each other and negatively associated with directional bias. This suggests that network-level phenomena may be mechanistically linked to tau strain identity. Below we discuss these findings in the context of the literature.

Potential mechanisms for net retrograde bias in tau propagation

The results of our statistical (**Figure 1**) and mathematical-modeling-based (**Figure 2** and **3**) analyses represent the first quantitative support for the possibility that a directional difference in the spread of tau pathology may be operative *in vivo*, or that this may have widespread consequences on the eventual pattern of progression within the brain. Most *in vivo* and *in vitro* studies indicate at least a bidirectional transmission of tau ***Dujardin et al.*** (***2014***); ***Iba et al.*** (***2013***); ***Tai et al.*** (***2014***); ***Wu et al.*** (***2013***). ***Iba et al.*** (***2013***) demonstrated the classic spread of preformed tau fibrils in P301S mouse model, and found that hippocampal seeding yields spread into entorhinal cortex (EC) and nearby cortices, raising the possibility that hippocampal efferents were involved. While these descriptive studies point to the plausibility of directional bias, here we present quantitative evidence across numerous experimental conditions that there is a notable, strain-specific retrograde bias in tau spreading. If confirmed by future bench studies, this finding has the potential to alter how we think about tau pathology progression.

We advance several potential mechanisms that may lead to this bias, building upon the hypothetical "molecular nexopathy" framework of degenerative diseases ***Warren et al.*** (***2013***). First, retrograde bias in tau pathology spread may be caused by progressive breakdown of the axon-soma barrier due to repeated exposure to hyperphosphorylated tau, leading to retrograde missorting of tau from axon to soma and dendrites ***Li et al.*** (***2011***). Because neuronal signaling and axon structural integrity become progressively degraded over the course of degenerative diseases ***Li et al.*** (***2011***), anterograde transynaptic transport likely becomes less frequent and more difficult. This would amount to a selection pressure towards misfolded tau strains that are more readily able to cross the synapse from dendritic bouton to axon terminal, thereby potentially leading to a retrograde bias across conditions. Aberrant tau conformations are also known to dysregulate energy-dependent transport of kinesin-1 ***Cuchillo-Ibanez et al.*** (***2008***); ***Rodríguez-Martín et al.*** (***2013***); ***Sherman et al.*** (***2016***); ***Stern et al.*** (***2017***), which leads to tau missorting over time and may underpin directional bias. This intriguing possibility has been explored mathematically in a two-neuron system ***Torok et al.*** (***2021***), but further exploration of the implications of transport breakdown and

network directional bias is required to draw firm conclusions.

Retrograde transmission of tau might also be mediated by amyloid-β (Aβ), which is known to induce early missorting of tau from axons to dendrites ***Ballatore et al.*** (***2007***); ***Fein et al.*** (***2008***); ***Ittner et al.*** (***2010***); ***Takahashi et al.*** (***2010***). Intracerebral Aβ injections in P301L transgenic mice exacerbated hyperphosphorylation of tau and NFT formation, not at somatosensory cortical and hippocampcal injection sites, but rather in the retrogradely-connected basolateral amygdala ***Götz et al.*** (***2001***). This suggests that Aβ induced damage to terminals or axons projecting to the injection site caused NFT formation in presynaptic cell bodies. While we lacked sufficient data to explore whether Aβ influences directionality in mouse tauopathy models, the fact that primary tauopathies (such as frontolobartemporal dementia, FTLD) and secondary tauopathies (such as AD) exhibit different etiologies suggests that Aβ may influence how tau spreads on the network. These explanations also need not be mutually exclusive: Aβ-induced retrograde tau transmission should appear earlier in the disease course than retrograde spread caused by the breakdown of the axon-soma barrier, as amyloidopathy has been repeatedly shown to precede or co-occur with tauopathy in AD ***Bolmont et al.*** (***2007***); ***Götz et al.*** (***2004***); ***Ittner et al.*** (***2010***).

Directional bias is strain-specific

It is well known that tau tangle structures within disease condition are often consistent, while they can vary considerably between disease condition ***Clavaguera et al.*** (***2013***). For example, when tau pathology from a human AD patient is injected into a mouse, the structure of tangle aggregates in the mice mirrors that of the patient ***Clavaguera et al.*** (***2013***); furthermore, comorbid Aβ/tau mouse models can reproduce Braak staging of tauopathy in the absence of a seed ***Hurtado et al.*** (***2010***). We found that net directional bias appears to be dependent on tau strain in a study-specific manner (**Figure 3**). While the optimal directionality bias parameter values in the NexIS:fit-s models (s_{opt}) were on average retrograde across studies and timepoints, we note that there is significant variation between them (**Figure 3C** and **E**; **Table 1**).

We chose these studies in part because they all shared a P301S tau mutation, 10 of the 11 mouse models had a PS19 genetic background (the last, Hurtado, was a PS19/PDAPP bigenic mouse model), disentangling the effects of different tau strains from injection sites is more challenging. We posit that tau strain is the predominant factor here rather than seeding site based on several pieces of evidence. First, IbaHippInj and IbaStrInj, which were both obtained from the same study ***Iba et al.*** (***2013***), differ only in seeding locations and exhibit similar retrograde biases by s_{opt} (**Table 1**). Additionally, the 6 studies from Kaufman, *et al.* (DS4, DS6, DS6 110, DS7, DS9, and DS9 110) were all seeded in PS19 mice in the left CA1 region of the hippocampus, and therefore only differ in their injectates ***Kaufman et al.*** (***2016***) (**Table 1**). These all exhibit marked differences in how tau pathology evolves over time (**Figure S1**), and while most are predominantly nondirectional, DS9 exhibits retrograde character (s_{opt} = 0.64). While these data are merely suggestive, strain specificity has been noted elsewhere as a general feature underlying the diversity of tauopathic diseases ***Frost and Diamond*** (***2010***). In particular, gross tangle structure is different across diseases, with AD tau fibrils forming NFTs and pre-helical formations (PHFs), Pick's Disease tau forming Pick bodies (PBs), and progressive supranuclear palsy (PSP), corticobasal degeneration (CBD), and frontotemporal dementia (FTD) oligomers forming more abundant NFTs ***Clavaguera et al.*** (***2013***).

What differences in these properties may at explain such a difference in their preferred directions of trans-synaptic spread? Pathological tau species can bypass or move through the axon-soma barrier, which in the normal state limits retrograde misplacement of tau into somatodendritic compartment, on an isoform or strain specific basis ***Zempel et al.*** (***2017***). Thus, it could be that certain misfolded tau strains are more readily able to break through the barrier than others. We also found that spread and accumulation rates are inversely related to directional spread bias; therefore, more aggressive tau strains are more likely to travel nondirectionally (**Figure 4**). One possible explanation, returning to the known dysregulation of axonal transport by tau ***Cuchillo-Ibanez et al.*** (***2008***); ***Rodríguez-Martín et al.*** (***2013***); ***Sherman et al.*** (***2016***); ***Stern et al.*** (***2017***), is that

these more pathological strains may simply impede axonal transport to the point where the only relevant process governing tau migration inside the neuron is diffusion.

Implications

The finding that the directional bias is dependent on conformation of tau has two potential implications. First, as mentioned above, differences in the observed aggressiveness of disease onset and propagation appear to be associated with both differential directional biases and different tau conformations. Second, it may help explain why there is such a diversity of spatial patterning of various tauopathies. This line of reasoning suggests that directional bias may lead to different areas where tau eventually accumulates, which may in turn lead to differential selective regional vulnerability of different brain regions to different tauopathies. Already, clinical studies confirm that the two disease hallmarks, regional tau pathology and neurodegeneration, exhibit divergent spatiotemporal development patterns between conditions, pertaining to their 3R and 4R tau isoforms ***Higuchi et al.*** (***2002***) and sites of tau hyperphosphorylation ***Hanger et al.*** (***2009***), as are the brain regions showing early disease vulnerability ***Braak and Del Tredici*** (***2011***); ***Burrell et al.*** (***2016***). Other tauopathic conditions can manifest early pathology in the orbitofrontal cortex (OFC), the amygdala (AMY), nucleus accumbens (NAcc) and caudate nuclues (CN) ***Burrell et al.*** (***2016***); ***Chiba et al.*** (***2012***). Furthermore, recent clinical evidence has identified AD-specific phosphoepitopes of tau ***Janelidze et al.*** (***2020***); ***Palmqvist et al.*** (***2020***); ***Thijssen et al.*** (***2020***), suggesting that amyloid comorbidity in AD may influence the ways in which tau is posttranslationally modified, which in turn leads to distinct patterns of neurodegeneration relative to primary tauopathies. The differences in spatiotemporal protein progression may eventually lead to differences in symptomatic progression. Tying these effects to underlying changes in directional bias would constitute a highly parsimonious and unifying mechanistic explanation. Future studies in both experimental and simulation systems should interrogate the sources of diversity among different neurodegenerative pathologies.

Materials and Methods

Datasets

The data in the present study for creating the mouse connectivity network comes from the Allen Mouse Brain Connectivity Atlas (AMBCA). This connectome was derived using viral tracing and coregistered to the Common Coordinate Framework (CCF) ***Oh et al.*** (***2014***); in total, there were 426 regions spanning both hemispheres in the connectome used in this study (**Figure 1C**). While there are multiple ways to quantify the amount of connectivity between regions, we chose to use *total* connectivity, rather than normalizing by volume. For all modeling analyses, the connectome was min-max normalized across all region-pairs. By convention, this 426×426 connectivity matrix, C, is oriented such that each entry c_{ij} corresponds to the connectivity *from* region i *to* region j.

Regional tau pathology data came from several studies that had to satisfy several criteria: 1) quantification or semi-quantification was based on immunohistochemistry (IHC); 2) the mice had to have a P301S tau mutant background to avoid conflating background endogenous tau protein type with other analyses; 3) at least 40 brain regions had to be quantified; 4) at least 3 timepoints had to be quantified. We summarize the key features of the 11 mouse models (spanning 4 studies: ***Boluda et al.*** (***2015***); ***Hurtado et al.*** (***2010***); ***Iba et al.*** (***2013***); ***Kaufman et al.*** (***2016***)) in **Table 1**. Further information about each dataset or study used in the present article can be found in their respective publications.

For data derived from Boluda, *et al.*, Iba, *et al.*, and Kaufman, *et al*., regional tau burden was manually extracted from heat map figures displaying semi-quantified pathology regions ***Boluda et al.*** (***2015***); ***Iba et al.*** (***2013***); ***Kaufman et al.*** (***2016***). Data from Hurtado, *et al.* represents disease staging per region, more than quantified or semi-quantified regional pathology, but was derived from a supplementary data table ***Hurtado et al.*** (***2010***). Using the AIBS mouse reference atlas (https://mouse.brain-map.org/static/atlas) as an anatomic reference, we manually coregistered

these regional tau values into the CCF space of the AMBCA on a per-study basis.

All datasets used for the analyses in this study are available in our NexIS GitHub repository (https://github.com/Raj-Lab-UCSF/Nexis).

NDM and NexIS:global

The original Network Diffusion Model (NDM) developed by Raj, *et al.* posits that the *rate of change* in tau concentration in a given region is proportional to the tau concentration differences between all other regions with which it shares a connection ***Raj et al.*** (***2012***). For a two-region system, the rate of change in tau in region 1 is given by:

$$\frac{dx_1}{dt} = \beta c_{12}(x_2 - x_1), \tag{1}$$

where x_i is the tau concentration in region i, β is a global spread rate parameter, and c_{ij} is the connectivity density between regions i and j. When C is symmetric, $c_{ij} = c_{ji}$ and this equation represents a *graph diffusion* process. This can be generalized across all regions using the graph Laplacian, L, of C:

$$\frac{d\mathbf{x}}{dt} = -\beta L\mathbf{x}, \tag{2}$$

where $L = D - C$ and D is the diagonal degree matrix of C. **Equation 2** is a set of ordinary, linear differential equations and has an explicit solution given by:

$$\mathbf{x}(t) = \mathbf{x}(0)e^{-\beta Lt}. \tag{3}$$

The NexIS:global model proposed by Anand, *et al.* extends this framework to account for the global accumulation of tau over time, which it posits is a linear function of current tau concentration:

$$\frac{d\mathbf{x}}{dt} = (-\beta L + \alpha I)\mathbf{x}, \tag{4}$$

$$\mathbf{x}(t) = \mathbf{x}(0)e^{(-\beta L + \alpha I)t}, \tag{5}$$

where L is defined as above and I is the identity matrix.

NexIS:dir

The above framework was proposed and implemented for symmetric connectomes only; that is, when $c_{ij} \equiv c_{ji}$. This is particularly appropriate for network modeling of human pathology, since human connectomes are obtained using diffusion tensor imaging (DTI), which is unable to distinguish the polarity of white matter tracts in the brain. However, the AMBCA is fully directed, and therefore it need not be assumed that flows along connection c_{ij} are equivalent to those along c_{ji}. Here, we define two extreme cases for NexIS:dir: 1) *purely retrograde spread*, where *positive flow* from region j to region i occurs along c_{ij}; 2) *purely retrograde spread*, where *positive flow* from region j to region i occurs along c_{ji}. Mathematically, the two-region retrograde case is given by:

$$\frac{dx_1}{dt} = \beta c_{12}(x_2 - x_1) + \alpha x_1, \tag{6}$$

and the two-region anterograde case is given by:

$$\frac{dx_1}{dt} = \beta c_{21}(x_2 - x_1) + \alpha x_1, \tag{7}$$

As above, these generalize across the network using the graph Laplacian (**Equation 4**); however, the form of the Laplacian differs between these two cases:

$$L_{ret} = D_{col}(C) - C, \tag{8}$$

$$L_{ant} = D_{row}(C) - C^T = D_{col}(C^T) - C^T, \tag{9}$$

where D_{row} and D_{col} are the row and column degree operators, respectively. $D_{row}(C)$ produces a matrix where each diagonal entry is the *outgoing* degree of C and $D_{col}(C)$ produces a matrix where each diagonal entry is the *incoming* degree of C.

With NexIS:dir, we propose that directionally biased spread need not be *entirely* aligned in the anterograde or retrograde directions as in **Equations 8** and **9**. To accomplish this, we first define a new *directionally weighted* connectome, C_s, as follows:

$$C_s = sC + (1 - s)C^T, \tag{10}$$

Here, s is a proportionality constant weighting the contributions of C and C^T to the flows on the network, and is bounded between 0 and 1. It is clear by inspection that $C_1 = C$ and $C_0 = C^T$. The directional Laplacian, then, is simply:

$$L_s = D_{col}(C_s) - C_s. \tag{11}$$

Again, $L_1 = L_{ret}$ and $L_0 = L_{ant}$. Finally, the full NexIS:dir model is given by:

$$\frac{d\mathbf{x}}{dt} = (-\beta L_s + \alpha I)\mathbf{x}, \tag{12}$$

$$\mathbf{x}(t) = \mathbf{x}(0)e^{(-\beta L_s + \alpha I)t}. \tag{13}$$

We note one other special case of NexIS:dir: the case when $s = 0.5$. $C_{0.5} = 0.5(C + C^T)$, and therefore $c_{0.5,ij} = 0.5(c_{ij} + cji) = c_{0.5,ji}$ and $C_{0.5}$ is symmetric. Therefore, we define the nondirectional Laplacian $L_{nd} = L_{0.5}$, which is equivalent to the NexIS:global case (**Equation 4**).

We use NexIS:fit-s, NexIS:ret, NexIS:ant, and NexIS:nd throughout this study, where these are distinguished by the forms of the Laplacian that they use in **Equation 12** (L_s, L_{ret}, L_{ant}, and L_{nd}, respectively).

Parameter fitting

We fit all parameters of the NexIS:dir model using MATLAB's `fmincon` nonlinear optimization algorithm for each study individually. We utilized two different fitting schemes: 1) longitudinal fitting, where all available timepoints were fit simultaneously; and 2) per-timepoint fitting, where α was first fixed to its longitudinally fit value and then the remaining parameters were fit to each timepoint individually. There is a latent parameter, γ, representing the proportionality constant relating amount of tau injected into seeded regions and the tau density as quantified by IHC; this scale factor varies by experimental condition and is necessary for making any fit of α meaningful. It also prevents the fitting of α in a per-timepoint fashion, as there is an identifiability problem between α and γ when fitting only one timepoint from seed. Therefore, for per-timepoint fitting, γ was also fixed alongside α.

The regional data space differs from the regional connectome space (i.e., the CCF) and between studies; notably, not all regions of the CCF were quantified in any given study. We therefore simulated the spread of pathology on the CCF atlas, producing 426 × number-of-timepoint matrices of NexIS:dir predictions. To optimize the parameters for a given mouse model, we first coregistered these predictions into that model's specific data space and then assessed the cost. The cost function used was the Lin's Concordance Correlation Coefficient, as previously described ***Lin*** (***1989***); ***Anand et al.*** (***2022***).

Statistical analysis

All statistical analysis involved performing standard linear regressions, Pearson's correlation, and t-tests using in-built MATLAB functions. p-values were subjected to the Bonferroni correction where appropriate.

Visualization

All analysis figures were produced using MATLAB plotting functions. The glass brain visualizations were generated using an in-house tool, Brainframe (https://github.com/Raj-Lab-UCSF/Brainframe).

Code and data availability

The data and code for these analyses and figures can be found in the NexIS repository (https://github.com/Ra
Lab-UCSF/Nexis).

Acknowledgments

We would like to acknowledge the Allen Institute for Brain Science and in particular their mouse reference and connectivity atlas toolboxes and research teams. Without their exemplary contributions to neuroscience and neuroanatomy, the present work would not be possible. We would also like to acknowledge the Weill Cornell Neuroscience and Radiology Departments, as well as the Feil Family Brain and Mind Research Institute and the many people who generously support Weill Cornell. We would also like to acknowledge Pedro D. Maia of the University of Texas at Arlington, who was instrumental in the development of the NexIS model. AR and CM are supported by grants from the National Institutes of Health (R01NS092802).

Author Contributions

CM and AR designed the models, wrote the analysis code in MATLAB, and co-wrote the manuscript. CM performed the literature searches to find the previously published datasets or tables and figures used as the "empirical data" here, performed the analyses to collect results and designed the figures and tables. JT assisted with the analysis and the editing of the manuscript.

Compliance with ethical standards

Conflict of interest: The authors declare no competing financial interests. Ethical approval and consent to participate: All mouse-work datasets in the present work was obtained from datasets originally presented in or with other already published work already declaring that all animal work was done under approved protocols and animal care standards.

References

Ahmed Z, Cooper J, Murray TK, Garn K, McNaughton E, Clarke H, Parhizkar S, Ward MA, Cavallini A, Jackson S, Bose S, Clavaguera F, Tolnay M, Lavenir I, Goedert M, Hutton ML, O'Neill MJ. A novel in vivo model of tau propagation with rapid and progressive neurofibrillary tangle pathology: the pattern of spread is determined by connectivity, not proximity. Acta Neuropathologica. 2014 may; 127(5):667–683. https://link.springer.com/10.1007/s00401-014-1254-6, doi: 10.1007/s00401-014-1254-6.

Anand C, Maia PD, Torok J, Mezias C, Raj A. The effects of microglia on tauopathy progression can be quantified using Nexopathy in silico (Nexis) models. Scientific Reports. 2022 dec; 12(1):21170. https://www.nature.com/articles/s41598-022-25131-3, doi: 10.1038/s41598-022-25131-3.

Ballatore C, Lee VMY, Trojanowski JQ. Tau-mediated neurodegeneration in Alzheimer's disease and related disorders. Nature Reviews Neuroscience. 2007 sep; 8(9):663–672. http://www.nature.com/articles/nrn2194, doi: 10.1038/nrn2194.

Bertsch M, Franchi B, Tesi MC, Tora V. The role of Abeta and Tau proteins in Alzheimer's disease: a mathematical model on graphs. Journal of Mathematical Biology. 2023 sep; 87(3):49. https://link.springer.com/10.1007/s00285-023-01985-7, doi: 10.1007/s00285-023-01985-7.

Bolmont T, Clavaguera F, Meyer-Luehmann M, Herzig MC, Radde R, Staufenbiel M, Lewis J, Hutton M, Tolnay M, Jucker M. Induction of Tau Pathology by Intracerebral Infusion of Amyloid-β-Containing Brain Extract and by Amyloid-β Deposition in APP × Tau Transgenic Mice. The American Journal of Pathology. 2007 dec; 171(6):2012–2020. https://linkinghub.elsevier.com/retrieve/pii/S0002944010624613, doi: 10.2353/ajpath.2007.070403.

Boluda S, Iba M, Zhang B, Raible KM, Lee VMY, Trojanowski JQ. Differential induction and spread of tau pathology in young PS19 tau transgenic mice following intracerebral injections of pathological tau from Alzheimer's disease or corticobasal degeneration brains. Acta Neuropathologica. 2015 feb; 129(2):221–237. http://link.springer.com/10.1007/s00401-014-1373-0, doi: 10.1007/s00401-014-1373-0.

Braak H, Braak E. Neuropathological stageing of Alzheimer-related changes. Acta Neuropathologica. 1991; 82:239–259. doi: 10.1007/BF00308809.

Braak H, Del Tredici K. Alzheimer's pathogenesis: is there neuron-to-neuron propagation? Acta Neuropathologica. 2011 may; 121(5):589–595. http://link.springer.com/10.1007/s00401-011-0825-z, doi: 10.1007/s00401-011-0825-z.

Burrell JR, Halliday GM, Kril JJ, Ittner LM, Götz J, Kiernan MC, Hodges JR. The frontotemporal dementia-motor neuron disease continuum. The Lancet. 2016 aug; 388(10047):919–931. https://linkinghub.elsevier.com/retrieve/pii/S0140673616007376, doi: 10.1016/S0140-6736(16)00737-6.

Chiba S, Takada E, Tadokoro M, Taniguchi T, Kadoyama K, Takenokuchi M, Kato S, Suzuki N. Loss of dopaminoreceptive neuron causes L-dopa resistant parkinsonism in tauopathy. Neurobiology of Aging. 2012 oct; 33(10):2491–2505. https://linkinghub.elsevier.com/retrieve/pii/S0197458011004738, doi: 10.1016/j.neurobiolaging.2011.11.002.

Clavaguera F, Akatsu H, Fraser G, Crowther RA, Frank S, Hench J, Probst A, Winkler DT, Reichwald J, Staufenbiel M, Ghetti B, Goedert M, Tolnay M. Brain homogenates from human tauopathies induce tau inclusions in mouse brain. Proceedings of the National Academy of Sciences. 2013 jun; 110(23):9535–9540. https://pnas.org/doi/full/10.1073/pnas.1301175110, doi: 10.1073/pnas.1301175110.

Clavaguera F, Bolmont T, Crowther RA, Abramowski D, Frank S, Probst A, Fraser G, Stalder AK, Beibel M, Staufenbiel M, Jucker M, Goedert M, Tolnay M. Transmission and spreading of tauopathy in transgenic mouse brain. Nature Cell Biology. 2009; doi: 10.1038/ncb1901.

Cuchillo-Ibanez I, Seereeram A, Byers HL, Leung K, Ward MA, Anderton BH, Hanger DP. Phosphorylation of tau regulates its axonal transport by controlling its binding to kinesin. The FASEB Journal. 2008 sep; 22(9):3186–3195. https://onlinelibrary.wiley.com/doi/10.1096/fj.08-109181, doi: 10.1096/fj.08-109181.

Dujardin S, Lécolle K, Caillierez R, Bégard S, Zommer N, Lachaud C, Carrier S, Dufour N, Aurégan G, Winderickx J, Hantraye P, Déglon N, Colin M, Buée L. Neuron-to-neuron wild-type Tau protein transfer through a trans-synaptic mechanism: relevance to sporadic tauopathies. Acta Neuropathologica Communications. 2014 dec; 2(1):14. https://actaneurocomms.biomedcentral.com/articles/10.1186/2051-5960-2-14, doi: 10.1186/2051-5960-2-14.

Fein JA, Sokolow S, Miller CA, Vinters HV, Yang F, Cole GM, Gylys KH. Co-Localization of Amyloid Beta and Tau Pathology in Alzheimer's Disease Synaptosomes. The American Journal of Pathology. 2008 jun; 172(6):1683–1692. https://linkinghub.elsevier.com/retrieve/pii/S0002944010619268, doi: 10.2353/ajpath.2008.070829.

Frost B, Diamond MI. Prion-like mechanisms in neurodegenerative diseases. Nature Reviews Neuroscience. 2010 mar; 11(3):155–159. http://www.nature.com/articles/nrn2786, doi: 10.1038/nrn2786.

Götz J, Chen F, van Dorpe J, Nitsch RM. Formation of Neurofibrillary Tangles in P301L Tau Transgenic Mice Induced by Aβ42 Fibrils. Science. 2001 aug; 293(5534):1491–1495. https://www.science.org/doi/10.1126/science.1062097, doi: 10.1126/science.1062097.

Götz J, Schild A, Hoerndli F, Pennanen L. Amyloid-induced neurofibrillary tangle formation in Alzheimer's disease: insight from transgenic mouse and tissue-culture models. International Journal of Developmental Neuroscience. 2004 nov; 22(7):453–465. https://onlinelibrary.wiley.com/doi/abs/10.1016/j.ijdevneu.2004.07.013, doi: 10.1016/j.ijdevneu.2004.07.013.

Hanger DP, Anderton BH, Noble W. Tau phosphorylation: the therapeutic challenge for neurodegenerative disease. Trends in Molecular Medicine. 2009 mar; 15(3):112–119. https://linkinghub.elsevier.com/retrieve/pii/S1471491409000331, doi: 10.1016/j.molmed.2009.01.003.

Higuchi M, Trojanowski JQ, Lee VMY. Tau Protein and Tauopathy. In: Davis KL, Charney D, Coyle JT, Nemeroff C, editors. *Neuropsychopharmacology: The Fifth Generation of Progress*, 5 ed. Philadelphia, PA, USA: Lippincott Williams and Wilkins; 2002.p. 1339–1354.

Holmes BB, Furman JL, Mahan TE, Yamasaki TR, Mirbaha H, Eades WC, Belaygorod L, Cairns NJ, Holtzman DM, Diamond MI. Proteopathic tau seeding predicts tauopathy in vivo. Proceedings of the National Academy of Sciences. 2014 oct; 111(41):E4376–E4385. http://www.pnas.org/cgi/doi/10.1073/pnas.1411649111, doi: 10.1073/pnas.1411649111.

Hurtado DE, Molina-Porcel L, Iba M, Aboagye AK, Paul SM, Trojanowski JQ, Lee VMY. Aβ Accelerates the Spatiotemporal Progression of Tau Pathology and Augments Tau Amyloidosis in an Alzheimer Mouse Model. The American Journal of Pathology. 2010 oct; 177(4):1977–1988. https://linkinghub.elsevier.com/retrieve/pii/S0002944010602489, doi: 10.2353/ajpath.2010.100346.

Iba M, Guo JL, McBride JD, Zhang B, Trojanowski JQ, Lee VMY. Synthetic Tau Fibrils Mediate Transmission of Neurofibrillary Tangles in a Transgenic Mouse Model of Alzheimer's-Like Tauopathy. Journal of Neuroscience. 2013 jan; 33(3):1024–1037. https://www.jneurosci.org/lookup/doi/10.1523/JNEUROSCI.2642-12.2013, doi: 10.1523/JNEUROSCI.2642-12.2013.

Iba M, McBride JD, Guo JL, Zhang B, Trojanowski JQ, Lee VMY. Tau pathology spread in PS19 tau transgenic mice following locus coeruleus (LC) injections of synthetic tau fibrils is determined by the LC's afferent and efferent connections. Acta Neuropathologica. 2015 sep; 130(3):349–362. http://link.springer.com/10.1007/s00401-015-1458-4, doi: 10.1007/s00401-015-1458-4.

Ittner LM, Ke YD, Delerue F, Bi M, Gladbach A, van Eersel J, Wölfing H, Chieng BC, Christie MJ, Napier IA, Eckert A, Staufenbiel M, Hardeman E, Götz J. Dendritic Function of Tau Mediates Amyloid-β Toxicity in Alzheimer's Disease Mouse Models. Cell. 2010 aug; 142(3):387–397. https://linkinghub.elsevier.com/retrieve/pii/S0092867410007269, doi: 10.1016/j.cell.2010.06.036.

Iturria-Medina Y. Anatomical Brain Networks on the Prediction of Abnormal Brain States. Brain Connectivity. 2013 feb; 3(1):1–21. http://www.liebertpub.com/doi/10.1089/brain.2012.0122, doi: 10.1089/brain.2012.0122.

Janelidze S, Mattsson N, Palmqvist S, Smith R, Beach TG, Serrano GE, Chai X, Proctor NK, Eichenlaub U, Zetterberg H, Blennow K, Reiman EM, Stomrud E, Dage JL, Hansson O. Plasma P-tau181 in Alzheimer's disease: relationship to other biomarkers, differential diagnosis, neuropathology and longitudinal progression to Alzheimer's dementia. Nature Medicine. 2020 mar; 26(3):379–386. http://www.nature.com/articles/s41591-020-0755-1, doi: 10.1038/s41591-020-0755-1.

Kaufman SK, Sanders DW, Thomas TL, Ruchinskas AJ, Vaquer-Alicea J, Sharma AM, Miller TM, Diamond MI. Tau Prion Strains Dictate Patterns of Cell Pathology, Progression Rate, and Regional Vulnerability In Vivo. Neuron. 2016 nov; 92(4):796–812. https://linkinghub.elsevier.com/retrieve/pii/S0896627316306973, doi: 10.1016/j.neuron.2016.09.055.

Kaufman SK, Thomas TL, Del Tredici K, Braak H, Diamond MI. Characterization of tau prion seeding activity and strains from formaldehyde-fixed tissue. Acta neuropathologica communications. 2017; doi: 10.1186/s40478-017-0442-8.

Langer Horvat L, Španić Popovački E, Babić Leko M, Zubčić K, Horvat L, Mustapić M, Hof PR, Šimić G. Anterograde and Retrograde Propagation of Inoculated Human Tau Fibrils and Tau Oligomers in a Non-Transgenic Rat Tauopathy Model. Biomedicines. 2023 mar; 11(4):1004. https://www.mdpi.com/2227-9059/11/4/1004, doi: 10.3390/biomedicines11041004.

Li X, Kumar Y, Zempel H, Mandelkow EM, Biernat J, Mandelkow E. Novel diffusion barrier for axonal retention of Tau in neurons and its failure in neurodegeneration. The EMBO Journal. 2011 nov; 30(23):4825–4837. http://emboj.embopress.org/cgi/doi/10.1038/emboj.2011.376, doi: 10.1038/emboj.2011.376.

Lin LIK. A Concordance Correlation Coefficient to Evaluate Reproducibility. Biometrics. 1989 mar; 45:255–268. https://www.jstor.org/stable/2532051?origin=crossref, doi: 10.2307/2532051.

Mezias C, LoCastro E, Xia C, Raj A. Connectivity, not region-intrinsic properties, predicts regional vulnerability to progressive tau pathology in mouse models of disease. Acta neuropathologica communications. 2017; 5(1). doi: 10.1186/s40478-017-0459-z.

Oh SW, Harris JA, Ng L, Winslow B, Cain N, Mihalas S, Wang Q, Lau C, Kuan L, Henry AM, Mortrud MT, Ouellette B, Nguyen TN, Sorensen SA, Slaughterbeck CR, Wakeman W, Li Y, Feng D, Ho A, Nicholas E, et al. A mesoscale connectome of the mouse brain. Nature. 2014 apr; 508(7495):207–214. http://www.nature.com/articles/nature13186, doi: 10.1038/nature13186.

Palmqvist S, Janelidze S, Quiroz YT, Zetterberg H, Lopera F, Stomrud E, Su Y, Chen Y, Serrano GE, Leuzy A, Mattsson-Carlgren N, Strandberg O, Smith R, Villegas A, Sepulveda-Falla D, Chai X, Proctor NK, Beach TG, Blennow K, Dage JL, et al. Discriminative Accuracy of Plasma Phospho-tau217 for Alzheimer Disease vs Other Neurodegenerative Disorders. JAMA. 2020 aug; 324(8):772. https://jamanetwork.com/journals/jama/fullarticle/2768841, doi: 10.1001/jama.2020.12134.

Raj A, Kuceyeski A, Weiner M. A Network Diffusion Model of Disease Progression in Dementia. Neuron. 2012 mar; 73(6):1204–1215. http://www.sciencedirect.com/science/article/pii/S0896627312001353http://www.cell.com/neuron/fulltext/S0896-6273(12)00135-3.

Raj A, LoCastro E, Kuceyeski A, Tosun D, Relkin N, Weiner M. Network Diffusion Model of Progression Predicts Longitudinal Patterns of Atrophy and Metabolism in Alzheimer's Disease. Cell Reports. 2015 jan; 10(3):359–369. https://linkinghub.elsevier.com/retrieve/pii/S2211124714010638, doi: 10.1016/j.celrep.2014.12.034.

Rodríguez-Martín T, Cuchillo-Ibáñez I, Noble W, Nyenya F, Anderton BH, Hanger DP. Tau phosphorylation affects its axonal transport and degradation. Neurobiology of Aging. 2013 sep; 34(9):2146–2157. https://linkinghub.elsevier.com/retrieve/pii/S0197458013001152, doi: 10.1016/j.neurobiolaging.2013.03.015.

Scholz T, Mandelkow E. Transport and diffusion of Tau protein in neurons. Cellular and Molecular Life Sciences. 2014 aug; 71(16):3139–3150. http://link.springer.com/10.1007/s00018-014-1610-7, doi: 10.1007/s00018-014-1610-7.

Sherman MA, LaCroix M, Amar F, Larson ME, Forster C, Aguzzi A, Bennett DA, Ramsden M, Lesne SE. Soluble Conformers of A and Tau Alter Selective Proteins Governing Axonal Transport. Journal of Neuroscience. 2016 sep; 36(37):9647–9658. https://www.jneurosci.org/lookup/doi/10.1523/JNEUROSCI.1899-16.2016, doi: 10.1523/JNEUROSCI.1899-16.2016.

Stern JL, Lessard DV, Hoeprich GJ, Morfini GA, Berger CL. Phosphoregulation of Tau modulates inhibition of kinesin-1 motility. Molecular Biology of the Cell. 2017 apr; 28(8):1079–1087. https://www.molbiolcell.org/doi/10.1091/mbc.e16-10-0728, doi: 10.1091/mbc.e16-10-0728.

Tai HC, Wang BY, Serrano-Pozo A, Frosch MP, Spires-Jones TL, Hyman BT. Frequent and symmetric deposition of misfolded tau oligomers within presynaptic and postsynaptic terminals in Alzheimer's disease. Acta Neuropathologica Communications. 2014 dec; 2(1):146. https://actaneurocomms.biomedcentral.com/articles/10.1186/s40478-014-0146-2, doi: 10.1186/s40478-014-0146-2.

Takahashi RH, Capetillo-Zarate E, Lin MT, Milner TA, Gouras GK. Co-occurrence of Alzheimer's disease β-amyloid and tau pathologies at synapses. Neurobiology of Aging. 2010 jul; 31(7):1145–1152. https://linkinghub.elsevier.com/retrieve/pii/S0197458008002777, doi: 10.1016/j.neurobiolaging.2008.07.021.

Thijssen EH, La Joie R, Wolf A, Strom A, Wang P, Iaccarino L, Bourakova V, Cobigo Y, Heuer H, Spina S, VandeVrede L, Chai X, Proctor NK, Airey DC, Shcherbinin S, Duggan Evans C, Sims JR, Zetterberg H, Blennow K, Karydas AM, et al. Diagnostic value of plasma phosphorylated tau181 in Alzheimer's disease and frontotemporal lobar degeneration. Nature Medicine. 2020 mar; 26(3):387–397. http://www.nature.com/articles/s41591-020-0762-2, doi: 10.1038/s41591-020-0762-2.

Torok J, Maia PD, Verma P, Mezias C, Raj A. Emergence of directional bias in tau deposition from axonal transport dynamics. PLOS Computational Biology. 2021 jul; 17(7):e1009258. https://dx.plos.org/10.1371/journal.pcbi.1009258, doi: 10.1371/journal.pcbi.1009258.

Warren JD, Rohrer JD, Schott JM, Fox NC, Hardy J, Rossor MN. Molecular nexopathies: a new paradigm of neurodegenerative disease. Trends in Neurosciences. 2013 oct; 36(10):561–569. https://linkinghub.elsevier.com/retrieve/pii/S0166223613001288, doi: 10.1016/j.tins.2013.06.007.

Weickenmeier J, Kuhl E, Goriely A. Multiphysics of Prionlike Diseases: Progression and Atrophy. Physical Review Letters. 2018; doi: 10.1103/PhysRevLett.121.158101.

Wu JW, Herman M, Liu L, Simoes S, Acker CM, Figueroa H, Steinberg JI, Margittai M, Kayed R, Zurzolo C, Di Paolo G, Duff KE. Small Misfolded Tau Species Are Internalized via Bulk Endocytosis and Anterogradely and Retrogradely Transported in Neurons. Journal of Biological Chemistry. 2013 jan; 288(3):1856–1870. https://linkinghub.elsevier.com/retrieve/pii/S0021925820465998, doi: 10.1074/jbc.M112.394528.

Zempel H, Dennissen FJA, Kumar Y, Luedtke J, Biernat J, Mandelkow EM, Mandelkow E. Axodendritic sorting and pathological missorting of Tau are isoform-specific and determined by axon initial segment architecture. Journal of Biological Chemistry. 2017; doi: 10.1074/jbc.M117.784702.

Zhou J, Gennatas ED, Kramer JH, Miller BL, Seeley WW. Predicting regional neurodegeneration from the healthy brain functional connectome. Neuron. 2012 mar; 73(6):1216–27. http://www.ncbi.nlm.nih.gov/pubmed/22445348http://www.pubmedcentral.nih.gov/articlerender.fcgi?artid=PMC3361461, doi: 10.1016/j.neuron.2012.03.004.

Figures and Tables

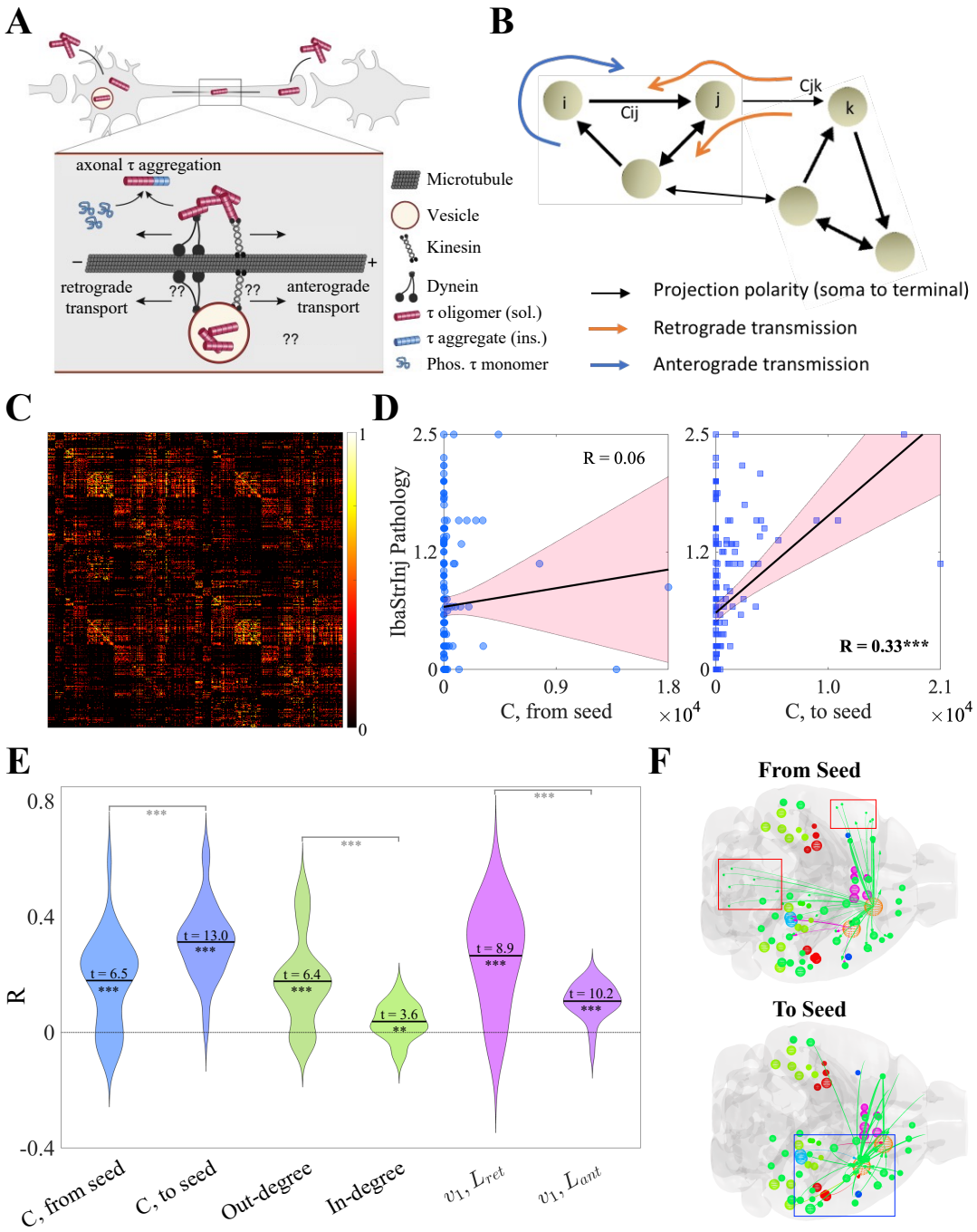
A
axonal τ aggregation
retrograde transport
anterograde transport
??
Microtubule
Vesicle
Kinesin
Dynein
τ oligomer (sol.)
τ aggregate (ins.)
Phos. τ monomer
B
i
j
k
Cij
Cjk
Projection polarity (soma to terminal)
Retrograde transmission
Anterograde transmission
C
D
IbaStrInj Pathology
R = 0.06
R = 0.33***
C, from seed
C, to seed
×10^4
E
R
t = 6.5
t = 13.0
t = 6.4
t = 3.6
t = 8.9
t = 10.2
C, from seed
C, to seed
Out-degree
In-degree
v_1, L_{ret}
v_1, L_{ant}
F
From Seed
To Seed

Figure 1. Tau exhibits a network-level directional preference. A. & **B.** Schematics showing the etiology of directional spread bias at the microscopic and network levels. Inside of axons, pathological tau can migrate by passive diffusion or through energy-dependent directed transport either in the *anterograde* (parallel to axon polarity) or *retrograde* (antiparallel to axon polarity) directions (**A**). At a network level, this manifests as an *directionally biased* flow along the directed connectome **B**. By convention, c_{ij} indicates a connection originating in region i and terminating in region j, therefore a net flow from i to j along c_{ij} would be considered to be *anterograde-biased*. **C.** The Allen Mouse Brain Connectome Atlas (AMBCA) ***Oh et al.*** (***2014***) visualized as a heatmap. **D.** Scatterplots showing the associations between the regional end-timepoint (9 MPI) pathology in the IbaStrInj ***Iba et al.*** (***2013***) experiment (see **Table 1**) and the average connectivity from (*left*) and (*right*) seeded regions CP and MOp. Tau shows a highly significant association with incoming but not outgoing connectivity. **E.** Violin plots showing the associations between tau pathology across all studies and time points and three pairs of region-level graph metrics; from right to left: outgoing and incoming connectivity to seed, out- and in-degree, and the first eigenvectors (v_1) of L_{ret} and L_{ant} (see **Materials and Methods**). One-sample t-statistics were calculated for each metric and two-sample t-statistics were calculated for each metric pair. All t-statistics were highly significant. **F.** Glass brain visualizations of end-timepoint IbaStrInj pathology and connectivity from (*top*) and to (*bottom*) seed regions (orange spheres). The low association between outgoing seed connectivity is in part driven by strong contralateral telencephalic and ipsilateral hindbrain projections (red boxes), which do not exhibit significant tau pathology. By contrast, the seeded regions predominantly receive connectivity from ipsilateral forebrain regions, which do exhibit pronounced tau pathology (blue box). MPI – months post injection; CP – caudoputamen; MOp – primary motor cortex. * – $p < 0.05$; ** – $p < 0.01$; *** – $p < 0.001$.

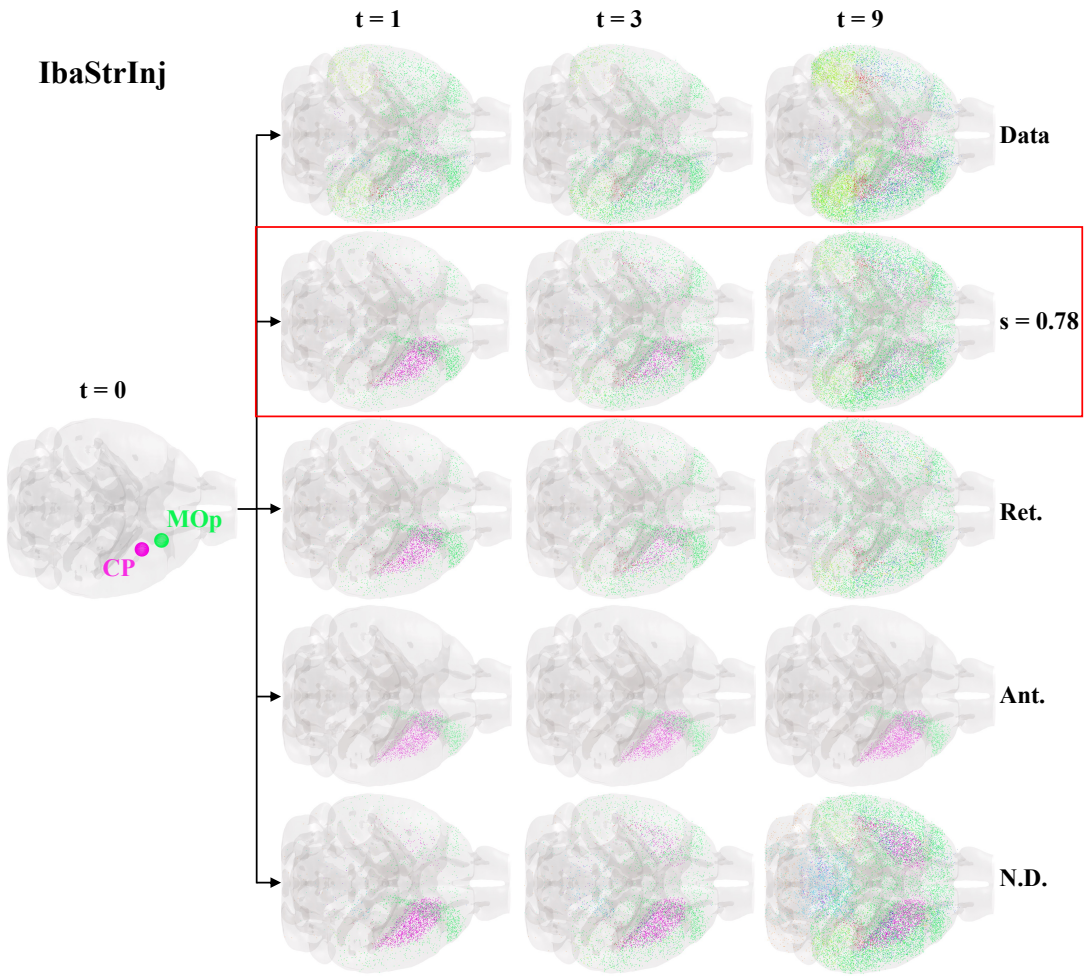

Figure 2. NexIS:dir models of IbaStrInj. Glass brain representations of the seed regions (CP and MOp) for the IbaStrInj experiment, visualized as spheres, and space-filling visualizations of regional tau pathology at the three quantified time points (t = 1, 3, and 9 MPI). The top row shows the observed tau distributions, with the predictions from four different NexIS:dir models shown below; in order from top to bottom: NexIS:fit-s (fitted $s = 0.78$), NexIS:ret (Ret.; $s = 1$), NexIS:ant (Ant.; $s = 0$), and NexIS:nd (N.D.; $s = 0.5$). While all models fail to capture the diffuse spreading of tau in IbaStrInj mice at 1 MPI, only by fitting the directionality bias parameter, s, does the model capture the distribution of tau at the last time point. Fitted $s = 0.78$ indicates mixed but retrograde-biased spread. CP – caudoputamen; MOp – primary motor cortex; Ret. – retrograde; Ant – anterograde; N.D. – nondirectional.

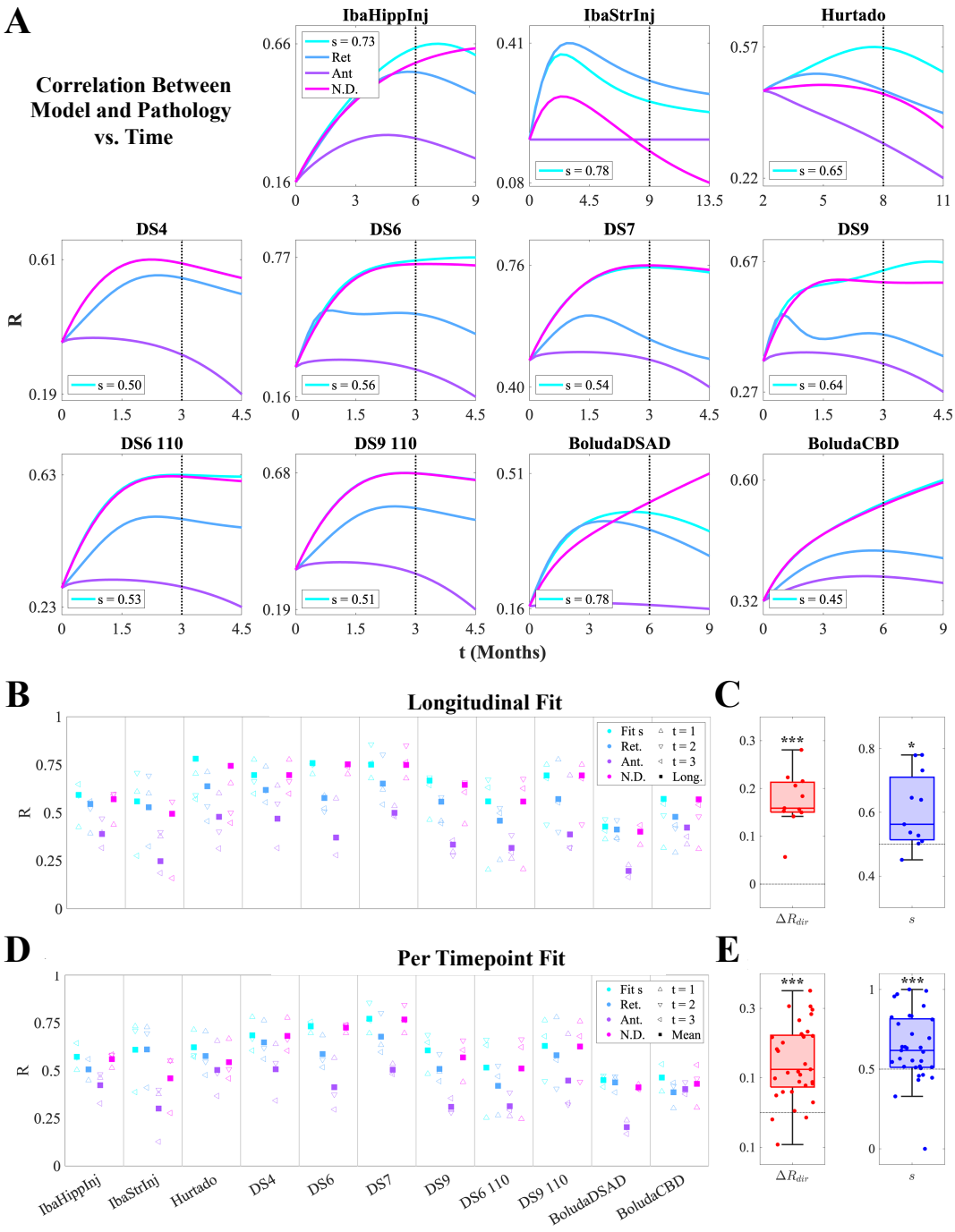
A
Correlation Between Model and Pathology vs. Time
IbaHippInj
IbaStrInj
Hurtado
DS4
DS6
DS7
DS9
DS6 110
DS9 110
BoludaDSAD
BoludaCBD
s = 0.73
Ret
Ant
N.D.
s = 0.78
s = 0.65
s = 0.50
s = 0.56
s = 0.54
s = 0.64
s = 0.53
s = 0.51
s = 0.78
s = 0.45
R
t (Months)
B
Longitudinal Fit
Fit s
Ret.
Ant.
N.D.
t = 1
t = 2
t = 3
Long.
C
***
*
ΔR_{dir}
s
D
Per Timepoint Fit
Fit s
Ret.
Ant.
N.D.
t = 1
t = 2
t = 3
Mean
IbaHippInj
IbaStrInj
Hurtado
DS4
DS6
DS7
DS9
DS6 110
DS9 110
BoludaDSAD
BoludaCBD
E
***
***
ΔR_{dir}
s

Figure 3. NexIS:dir model performance across all mouse experiments. **A.** Plots of Pearson's correlation (R) values between the predicted tau pathology using the four types of NexIS:dir models over time, and the observed tau pathology at the last quantified time point for each of the 11 experiments (dotted vertical lines). **B.** Per-timepoint (triangles) and overall (squares) R values for each of the four NexIS:dir models (NexIS:fit-s, NexIS:ret, NexIS:ant, and NexIS:nd) with respect to the observed tau distributions of each of the 11 mouse experiments, where each model's parameters were fit *longitudinally*. While NexIS:ret and NexIS:nd models often perform comparably well to NexIS:fit-s, NexIS:ant is always the worst-performing model overall. **C.** Boxplots of ΔR_{dir} ($R_{ret} - R_{ant}$; *left*) and fitted s values (*right*) across experiments, assessed for longitudinally fit models. Both metrics show an overall net retrograde spread bias. **D.** Per-timepoint (triangles) and mean across time (squares) R values for each of the four NexIS:dir models (NexIS:fit-s, NexIS:ret, NexIS:ant, and NexIS:nd) with respect to the observed tau distributions of each of the 11 mouse experiments, where each model's parameters were fit *to each timepoint individually*. Similar to **B**, NexIS:ant generally performs worse than all other models. **E.** Boxplots of ΔR_{dir} ($R_{ret} - R_{ant}$; *left*) and fitted s values (*right*) across experiments, assessed for per-timepoint fit models. As in **C**, both metrics show an overall net retrograde spread bias. * – $p < 0.05$; ** – $p < 0.01$; *** – $p < 0.001$.

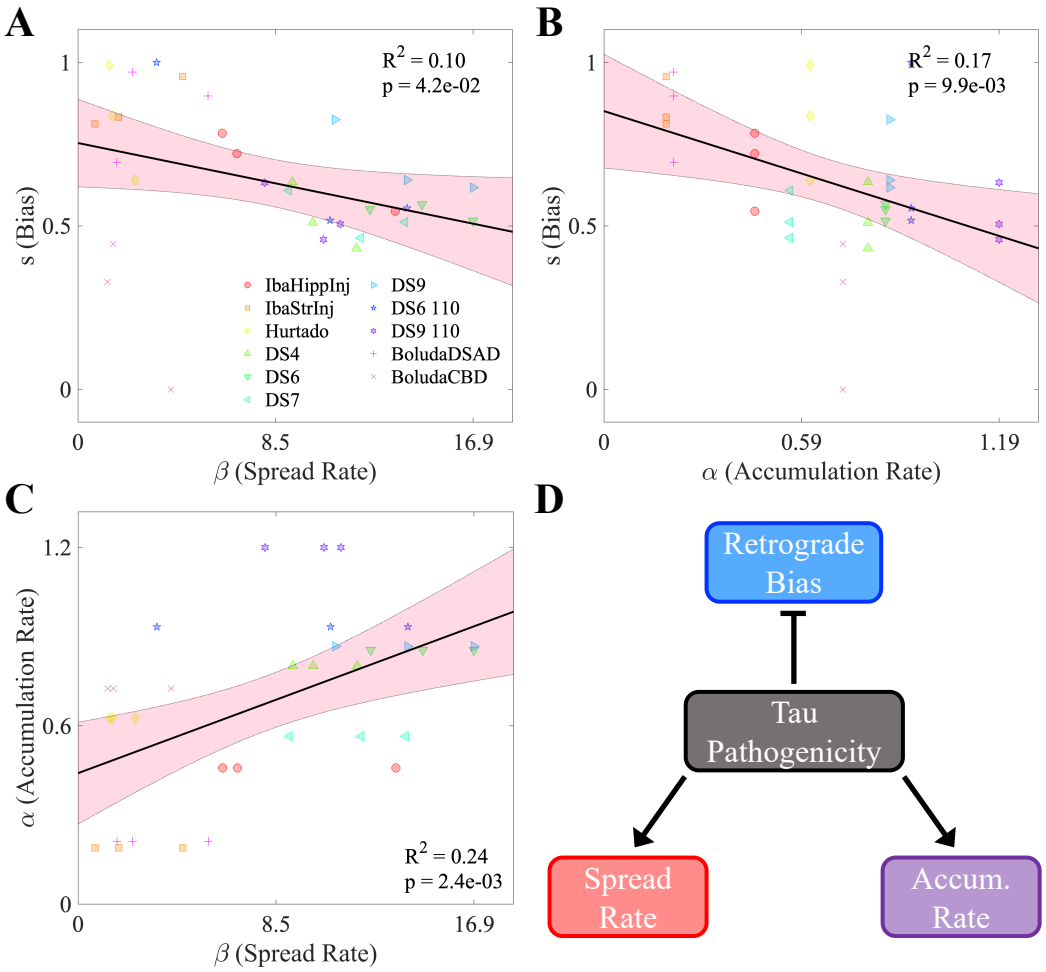

Figure 4. Interrelationships between NexIS:dir parameters. A. Scatterplot of fitted s values vs. spread rate parameter (β) values in the NexIS:fit-s model across all time points and experiments. Both parameters were fit individually per timepoint. There is a modest but statistically significant negative association between s and β ($p < 0.05$). **B.** Scatterplot of fitted s values vs. accumulation rate parameter (α) values in the NexIS:fit-s model across all time points and experiments. As in **A**, the s parameter was fit individually per timepoint, while $alpha$ was fit longitudinally and fixed across timepoints (see **Materials and Methods**). There is a moderately statistically significant association between s and α ($p < 0.01$). **C.** Scatterplot of α values vs. β values in the NexIS:fit-s model across all time points and experiments. The parameters were fit as in **A** and **B**. There is a moderately statistically significant association between α and β ($p < 0.01$). **D.** Proposed model for the interrelationships between these parameters. Overall tau pathogenicity is associated with higher accumulation and spread parameters, which are positively correlated, and is also associated with a transition from retrograde-biased to nondirectional spreading of tau along the connectome.

Name	Mouse Model Description	$R_{\text{fit-s}}$	s_{opt}
IbaStrInj ***Iba et al.*** (***2013***)	PS19 mice seeded with synthetic PFFs from 2N4R P301S tau (T40/PS) and from truncated P301L tau (K18/PL) in the right CP and right MOp	$\mathbf{0.56}^{***}$	0.78
IbaHippInj ***Iba et al.*** (***2013***)	PS19 mice seeded with synthetic PFFs from 2N4R P301S tau (T40/PS) and from truncated P301L tau (K18/PL) in the right DG	$\mathbf{0.59}^{***}$	0.73
Hurtado ***Hurtado et al.*** (***2010***)	Unseeded doubly transgenic PS19/PDAPP mouse	$\mathbf{0.78}^{***}$	0.65
DS4 ***Kaufman et al.*** (***2016***)	PS19 mice seeded with tau from AD brain homogenate in the left CA1 area	$\mathbf{0.70}^{***}$	0.50
DS6 ***Kaufman et al.*** (***2016***)	PS19 mice seeded with P301S mouse-derived, fibril-like cytoplasmic inclusions (“threads”) in the left CA1 area	$\mathbf{0.76}^{***}$	0.56
DS6 110 ***Kaufman et al.*** (***2016***)	PS19 mice seeded with a 1:10 dilution of the **DS6** tau strain in the left CA1 area	$\mathbf{0.56}^{***}$	0.53
DS7 ***Kaufman et al.*** (***2016***)	PS19 mice seeded with recombinant fibrils with prominent nuclear inclusions (“speckles”) in the left CA1 area	$\mathbf{0.75}^{***}$	0.54
DS9 ***Kaufman et al.*** (***2016***)	PS19 mice seeded with recombinant fibrils with prominent nuclear inclusions (“speckles”) in the left CA1 area	$\mathbf{0.67}^{***}$	0.64
DS9 110 ***Kaufman et al.*** (***2016***)	PS19 mice seeded with a 1:10 dilution of the **DS9** tau strain in the left CA1 area	$\mathbf{0.69}^{***}$	0.51
BoludaDSAD ***Boluda et al.*** (***2015***)	PS19 mice injected with DSAD brain homogenate in the left CA1 and left primary somatosensory areas (LH)	$\mathbf{0.43}^{***}$	0.78
BoludaCBD ***Boluda et al.*** (***2015***)	PS19 mice injected with CBD brain homogenate in the left CA1 and left primary somatosensory areas (LH)	$\mathbf{0.57}^{***}$	0.45

Table 1. Summary of key NexIS:directed results. List of the tauopathy datasets explored here with descriptions of each experiment’s mouse genetic background, injection site, and type of tau injected. The Pearson’s correlation values for the directionality-fitted models ($R_{\text{fit-s}}$) and the optimal directionality parameter (s_{opt}) values are provided. All studies were quantified tau pathology within hemispheres ipsilateral and contralateral to the injection site separately with the exception of Hurtado, which was bilaterally averaged. PFF – preformed fibrils; DSAD – Down Syndrome Alzheimer’s disease; CBD – corticobasal dengeneration. * – $p < 0.05$; ** – $p < 0.01$; *** – $p < 0.001$.